Available online at www.sciencedirect.com
SCIENCE DIRECT®
Acta Materialia 53 (2005) 2875–2880
Acta MATERIALIA
www.actamat-journals.com

Real-time observation of grain nucleation and growth during solidification of aluminium alloys

N. Iqbal [a], N.H. van Dijk [a,*], S.E. Offerman [b,a], M.P. Moret [c], L. Katgerman [b], G.J. Kearley [a]

[a] *Fundamental Aspects of Materials and Energy, Faculty of Applied Sciences, Delft University of Technology, Mekelweg 15, 2629 JB Delft, Netherlands*
[b] *Department of Materials Science and Engineering, Delft University of Technology, Rotterdamseweg 137, 2628 AL Delft, Netherlands*
[c] *European Synchrotron Radiation Facility, 6 Rue Jules Horowitz, BP 220, 38043 Grenoble Cedex 9, France*

Received 24 January 2005; received in revised form 10 February 2005; accepted 10 February 2005
Available online 20 April 2005

Abstract

The crystallisation kinetics of liquid aluminium–titanium alloys with microscopic TiB_2 particles added to refine the grain size in the solidified material was studied by X-ray diffraction measurements at a synchrotron source. Real-time observation of the formation and growth of individual grains reveals the central role played by the added TiB_2 particles during solidification. Prior to the main transformation, weak reflections of a metastable $TiAl_3$ phase were detected. This observation finally pinpoints the highly debated mechanism responsible for enhanced grain nucleation in Al–Ti–B alloys.

Keywords: Solidification; Grain refinement; X-ray diffraction; Aluminium alloys; TiB_2

1. Introduction

Liquid-to-solid phase transformations often form an essential step in the processing of polycrystalline materials. A detailed understanding of this phenomenon is of both fundamental interest and technological importance for the formation of many polycrystalline materials. During solidification two processes can be identified: grain nucleation and subsequent grain growth [1]. At the time of nucleation a small cluster of the solid phase, which fluctuates in size, reaches a dimension that can no longer remelt. During grain growth the stable nuclei increase in size until the material is completely solidified.

The current understanding of grain nucleation is still limited due to the experimental difficulty of monitoring the formation of relatively small nuclei in the bulk of the material and the computation resources needed to evaluate the stability of the fluctuating clusters in the melt. Recent advances in this field have come through laser confocal microscopy experiments [2] and numerical simulations [3] on the crystallisation behaviour of colloids. For liquid metals few experimental techniques are available to probe the nucleation and growth of individual grains within the melt. The recent development of X-ray diffraction microscopes at synchrotron sources with high-energy X-rays has created the opportunity to study individual grains in the bulk of a material [4–6]. In a recent study [7] this technique was used to probe both nucleation and growth of individual grains for a solid-state phase transformation within the bulk of a steel sample. The present X-ray diffraction study represents the first determination of the nucleation and growth behaviour of individual grains within the melt during solidification of a metal. The relatively high viscosity of the liquid metal with minimal grain rotations

* Corresponding author. Tel.: +31 15 27 86775; fax: +31 15 27 88303.
E-mail address: nvdijk@iri.tudelft.nl (N.H. van Dijk).

1359-6454/$30.00
doi:10.1016/j.actamat.2005.02.045

allowed us to monitor the complete growth of individual grains floating in the melt.

The mechanical properties of polycrystalline materials depend critically on the average grain size, and often improve as the average grain size is reduced. Generally, grain refinement in metals can be achieved by adding micron-sized particles to the melt [8]. These particles are thought to cause an enhanced nucleation of the solid grains on the surface of the added particles. The mechanism underlying this process of grain refinement with added particles is, however, still unclear [9–11]. In aluminium alloys with added TiB_2 particles it was found that grain refinement is only effective if a small concentration of solute titanium is added to the melt. However, for these small concentrations of solute titanium no additional phases, which could assist the nucleation of aluminium grains on the added particles, are expected to form according to the phase diagram. This controversy has lead to a wide variety of models being proposed to explain the influence of the solute titanium on the grain nucleation in these alloys. In this study, we demonstrate that a metastable phase plays a key role in the enhanced grain nucleation in liquid aluminium alloys. We directly observe that grain nucleation only occurs in the first stage of the transformation and that the grain growth initially follows the model prediction for diffusion-controlled growth without interactions between the grains.

2. Experimental

2.1. Sample preparation

The aluminium alloys were prepared from pure Al (99.999%) and Ti (99.99%) from Goodfellow, and TiB_2 (99.99%) from GE Advanced Ceramics. The Al and Ti were melted in the appropriate ratios in an arc furnace under high purity argon, solidified and remolten five times to obtain a homogeneous alloy. The solute concentration of 0.097(5) wt.% Ti in the alloy was determined by X-ray fluorescence spectroscopy. The TiB_2 particles with a size distribution between 3 and 6 μm and a maximum around 4.4 μm were then added to the reheated liquid metals and homogeneously distributed by stirring to prepare solid mixtures for the X-ray diffraction experiments. As the high purity TiB_2 particles were not heated before entering the melt we expect oxidation to be minimal. The relatively small size of the TiB_2 particles leads to a minimal effect of settling during the experiment.

2.2. Experimental procedure

X-ray diffraction measurements were performed using the three-dimensional X-ray diffraction microscope (3DXRD) at beam line ID11 of the European Synchrotron Radiation Facility in transmission geometry. The experimental set-up is shown in Fig. 1. A monochromatic X-ray beam with an energy of 70 keV (wavelength of 0.177 Å) and a beam size of 200×200 μm^2 illuminated the 5 mm diameter of the sample (with a height of 10 mm) that was mounted in a glassy carbon container within the vacuum furnace. A continuous sample rotation of 1° around the vertical axis (perpendicular to the beam) gives rise to a diffraction pattern on the two-dimensional detector that is placed behind the sample. This pattern gives direct information on both the liquid and solid phases during the solidification process.

In order to probe grain nucleation during solidification the beam size was enhanced from 200×200 μm^2 to 300×300 μm^2 on each alternate exposure in order to check that the grains nucleated in the smaller central beam. Reflections that first appeared during exposure with the larger beam were discarded as nucleation events because they cannot be distinguished from grains that nucleated outside the illuminated sample volume and grew into it.

In order to probe the grain radius of individual grains it is essential that the total grain volume is illuminated and the complete integrated intensity of the reflection is recorded. During the X-ray diffraction measurements four subsequent exposures were collected while the sample was continuously rotated around the vertical axis by 1° per exposure. In order to determine whether the complete integrated intensity was observed in one of the two central exposures, the intensity was compared to those of the two neighbouring rotation intervals. On alternate sets of exposures the beam size was enhanced from 200×200 μm^2 to 300×300 μm^2 to check that the total grain volume was illuminated by the smaller central beam. Only grains that fulfilled both conditions were considered [4]. The absolute size of the grain was determined by an internal calibration of the Bragg intensity

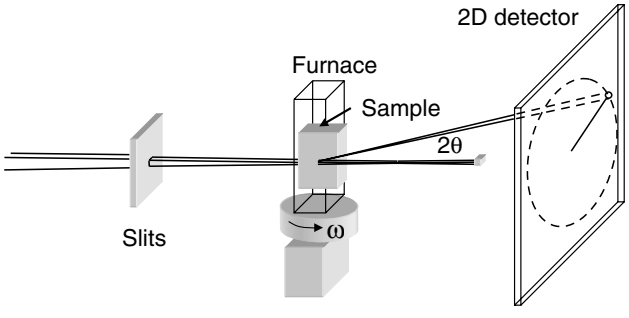

Fig. 1. Schematic outline of the experimental X-ray diffraction set-up. A monochromatic beam of hard X-rays defined by slits illuminates the sample mounted in a vacuum furnace. The diffracted intensity, scattered over an angle 2θ, is monitored by a two-dimensional detector while the sample is rotated over an angle ω around the vertical axis. The direct beam is shielded from the detector by a beam stop.

to the intensity of the first peak in the liquid structure factor.

3. Results and discussion

3.1. X-ray diffraction patterns

Fig. 2 shows the diffraction pattern of an aluminium-alloy with solute titanium and added TiB_2 particles at three stages during continuous cooling. In the liquid phase (Fig. 2(a)) two broad rings indicate the maxima in the liquid structure factor resulting from short-range order of the aluminium atoms. In the mixed phase (Fig. 2(b)) the intensity of the broad rings is reduced, and a limited number of diffraction spots from the solid grains is observed at the diffraction angles corresponding to reflections of the face-centred cubic lattice structure of aluminium. In the solid phase (Fig. 2(c)) the broad rings of the liquid phase are absent and the diffraction spots show an increase in number and intensity. According to standard diffraction theory the number of spots detected is proportional to the number of illuminated grains and the intensity of each spot is proportional to the volume of the grain from which it originates. The liquid phase fraction f_l, and consequently also the solid phase fraction $f_s = 1 - f_l$, can be determined accurately by scaling the intensity variation of the first diffuse ring of the liquid pattern at a part of the ring in which no diffraction spots of the solid phase appear. By repeated acquisition of images, the nucleation and growth of individual grains were studied with a typical time resolution of 8 s.

3.2. Grain nucleation

The aluminium alloys were kept for 30 min at 973 K (about 40 K above the melting temperature of aluminium) in order to form a homogeneous liquid phase, and were subsequently cooled at a rate of 1 and 10 K/min. In Fig. 3 the number of nucleated grains and the solid phase fraction is shown as a function of time for three aluminium alloys at different cooling rates. By counting the number of diffraction spots as a function of time, the evolution of the number of aluminium grains in reflection was obtained (for grains with a radius above the detection limit of about 2 μm for the main aluminium reflections). From all reflections on the detector only the grains that nucleated in the illuminated sample volume were considered and the grains that grew into it were discarded. The observed number of grains that fulfil the Bragg condition is proportional to the grain density (within a relative statistical uncertainty of $1/\sqrt{N}$). The corresponding solid phase fraction was determined from the scaled intensity at the first ring in the diffraction pattern of the liquid phase. When the final number of reflecting grains in Fig. 3 is compared for the different alloys, significantly more are found for the alloy containing both solute titanium and added microscopic TiB_2 particles. This clearly confirms that grain refinement is only effective when both solute titanium and added microscopic TiB_2 particles are present [9–11]. Further, our measurements in Fig. 3 demonstrate that the nucleation process is limited to the initial stage of the solidification and is complete at a solid phase fraction of about 20% for all samples. This remarkable observation indicates that the energy barrier for nucleation increases strongly after a considerable fraction of the solid phase fraction has been formed. According to the classical nucleation theory [12] the energy barrier for nucleation on a substrate ΔG^* corresponds to

$$\Delta G^* = \left(\frac{16\pi}{3}\right)\left(\frac{\sigma^3}{\Delta G_v^2}\right)F(\theta), \tag{1}$$

where σ is the energy of the new interface, $\Delta G_v \approx L\Delta T/T_m$ is the driving force of the nucleation, L is the latent heat, ΔT the undercooling below the liquidus temperature T_m, and $F(\theta)=(2+\cos\theta)(1-\cos\theta)^2/4$ is a function

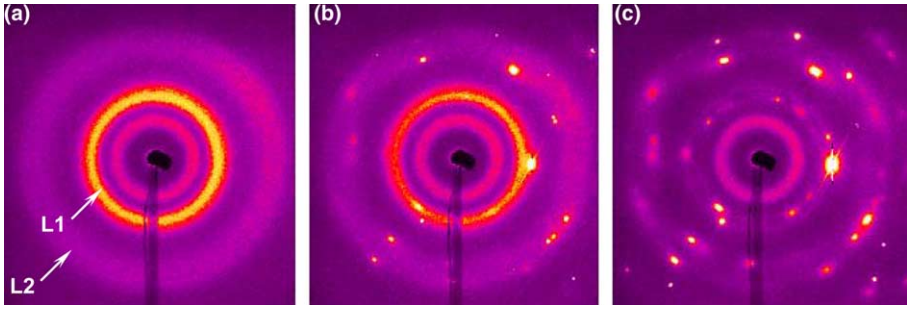

Fig. 2. X-ray diffraction patterns of the aluminium alloy with solute titanium (0.1 wt.%) and added TiB_2 particles (0.1 wt.%) at different stages of the solidification process. The data were collected during cooling from 973 K at a rate of 1 K/min. (a) In the liquid phase the two broad outer rings are due to the first (L1) and second (L2) maximum in the liquid structure factor. (b) In the mixed phase additional bright spots are Bragg reflections from nucleated grains at the scattering angles of the aluminium lattice structure. (c) In the solid phase the diffraction spots have increased in number and intensity while the diffuse scattering of the liquid phase has vanished. The diffuse innermost ring arises from the quartz windows of the vacuum furnace.

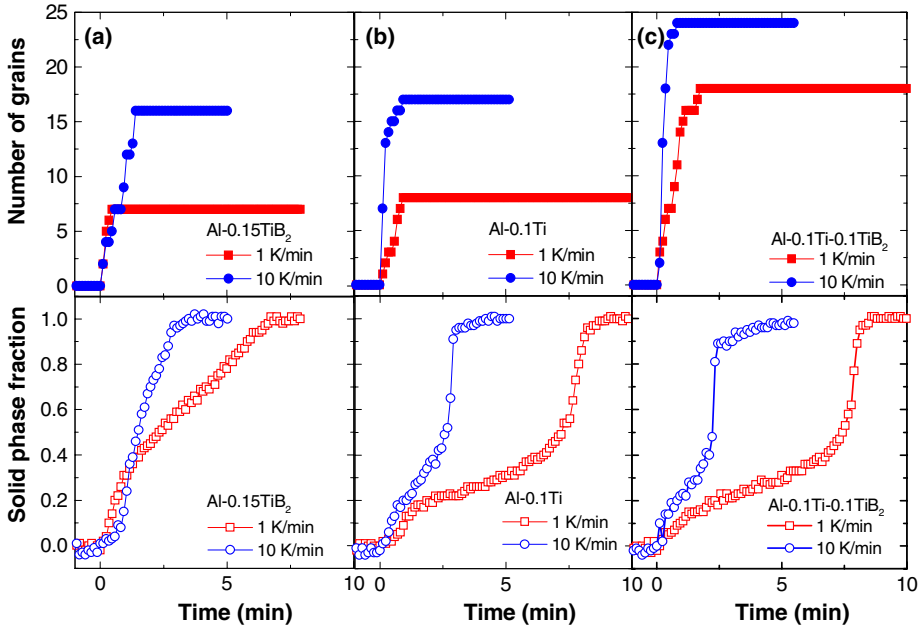

Fig. 3. Grain nucleation and solid phase fraction of three aluminium alloys as a function of time for different cooling rates. X-ray diffraction patterns were monitored as a function of time for aluminium alloys with (a) added TiB_2 particles (0.15 wt.%), (b) solute titanium (0.1 wt.%), and (c) both solute titanium (0.1 wt.%) and added TiB_2 particles (0.1 wt.%) during cooling from 973 K with a cooling rate of 1 and 10 K/min. The upper frames show the total number of nucleated grains in reflection (after validation that they nucleated in the illuminated sample volume). The lower frames show the corresponding solid phase fraction deduced from the scaled intensity variation in the first maximum of the liquid structure factor. The time, $t = 0$ min, corresponds to the onset of the solidification.

of the wetting angle, θ, between the solid phase and the substrate. The increase in the nucleation barrier during solidification is caused by an increase in the local sample temperature as latent heat is released [13]. For all samples the number of nuclei formed increases with cooling rate indicating that the maximum undercooling reached during solidification increases for higher cooling rates. As grain nucleation requires a minimum amount of undercooling to be effective, most potential nucleation sites become inactive when the temperature rises due to the release of latent heat from the previously nucleated grains. As a consequence, only a small fraction of the TiB_2 particles, which is controlled by the maximum undercooling and the wetting angle, actually nucleates a grain during the transformation. From the data in Fig. 3 we can further conclude, in agreement with previous studies [9–11], that an effective wetting of the TiB_2 substrate is only observed when solute titanium is present. The retarded growth caused by the diffusion of solute titanium is often thought to play an important role in the grain refinement as there is more time for nucleation events to occur [10,13]. Although a retarded grain growth in the presence of solute titanium indeed delays a recalescence and thereby increases the maximum undercooling reached for aluminium alloys with added TiB_2 particles, the grain nucleation was not found to extend over significantly longer times. Apparently, the enhanced grain nucleation is predominantly caused by the improved wetting of the TiB_2 substrate in the presence of solute titanium and to a lesser extent by a retarded growth.

3.3. Grain growth

The growth behaviour of individual aluminium grains during solidification was determined by monitoring the intensity of the diffraction spots continuously. In Fig. 4 the overall growth kinetics of the individual grains is shown for the alloys containing solute titanium with and without added TiB_2 particles. The individual growth curves show a close resemblance to the behaviour of the solid fraction. The observed growth behaviour of the individual grains is controlled by the diffusion of solute titanium and the release of latent heat. As titanium has a strong affinity for the solid phase, its concentration in the melt decreases as the solidification proceeds. For diffusion-controlled growth of non-interacting grains, the grain radius R as a function of time t is given by [14]:

$$R(t) = \lambda_s \sqrt{D_s(t - t_s)}, \quad (2)$$

where λ_s is a parameter that is determined from the titanium solubility in the liquid and the solid phases, D_s is the diffusion constant of solute titanium in the liquid [15], and t_s is the moment of nucleation of the grain. In the growth curves of the individual grains shown in Fig. 4, three different stages can be distinguished. In the first stage the individual growth curves are consistent with the model prediction for

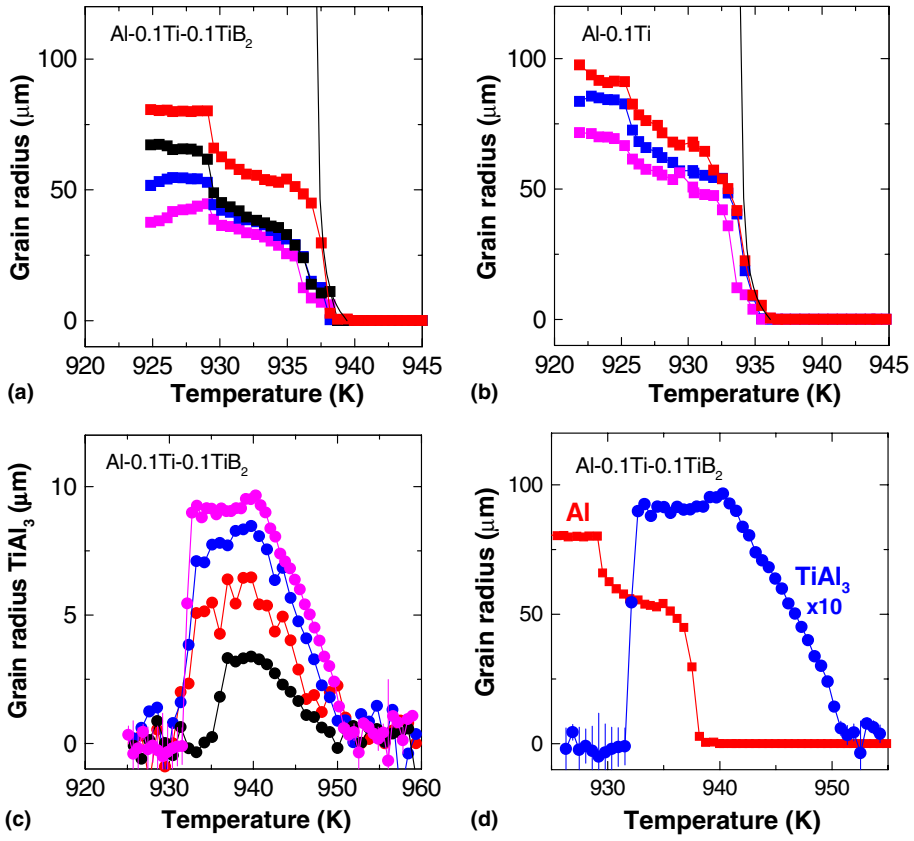

Fig. 4. Grain growth of individual aluminium and metastable $TiAl_3$ grains as a function of temperature for two aluminium alloys. The grain radius of individual aluminium grains is shown as a function of temperature during continuous cooling (1 K/min) from 973 K in (a) for the alloy with both solute titanium (0.1 wt.%) and added TiB_2 particles (0.1 wt.%) and in (b) for the alloy with only solute titanium (0.1 wt.%). The grain radius was deduced by assuming a spherical geometry. Solid lines indicate the model calculation for diffusion-controlled growth. The grain radius of individual $TiAl_3$ grains in the aluminium alloy with solute titanium and added TiB_2 particles is shown in (c) and compared to the growth of an individual aluminium grain in (d). The $TiAl_3$ grains nucleate about 10 K above the experimental onset of nucleation for aluminium grains, and become unstable when solid aluminium has formed.

diffusion-controlled growth of non-interacting grains. These observations are the first in situ confirmation that grain growth within the melt of a liquid metal initially obeys the widely applied model of Eq. (2). After this stage, the growth rate is reduced by an increase in temperature caused by the release of latent heat (and to a minor extend due to the indirect interaction of the growing grains via overlapping diffusion fields), leading to a reduced growth parameter λ_s. Near the end of the transformation the growth rate rapidly increases when the undercooling increases again during our continuous cooling experiment.

3.4. Metastable $TiAl_3$

A careful analysis of the measured diffraction patterns shows the presence of a limited number of weak diffraction spots (at a wave-vector transfer of $Q = 4.0$, 4.4, 5.6, and 6.3 Å^{-1}) in the alloy with solute titanium and added TiB_2 particles, which could not be indexed as aluminium grains. The most likely origin of these reflections in our high-purity alloy is the presence of a $TiAl_3$ phase (the spots then correspond to {1 0 5}, {2 0 4}, and {3 2 3} reflections of the tetragonal structure and to a {3 2 0} reflection of the metastable cubic structure). It is remarkable that these reflections (Fig. 4(c)) first appear about 10 K above the experimental solidification temperature of aluminium. At the nucleation temperature of the aluminium grains the intensity of the $TiAl_3$ reflections start to decrease, and finally vanish near the end of the transformation. The absence of these $TiAl_3$ reflections in the sample containing solute titanium without the added TiB_2 particles shows that the $TiAl_3$ phase plays an essential role in the enhanced nucleation process as revealed in Fig. 3. Apparently, the nucleation of $TiAl_3$ on the TiB_2 substrate is substantially more effective than the nucleation of aluminium. Indeed, one of the many mechanisms proposed to explain the enhanced nucleation in this system, the duplex nucleation theory [9–11], proposes that the TiB_2 particles need to be coated by a thin layer of $TiAl_3$ in order to be effective

nucleant particles. From earlier measurements it is known that once $TiAl_3$ is formed it acts as an excellent nucleation site for aluminium [16]. Our present in situ study shows that the TiB_2 substrates stabilise a $TiAl_3$ phase in a limited temperature range above the solidification temperature of aluminium. This formation of a $TiAl_3$ phase in aluminium alloys with a titanium concentration below 0.15 wt.%, where it is considered unstable according to the Al–Ti phase diagram, has long been proposed but was so far not supported by experimental evidence due to the lack of in situ data [10,11].

4. Conclusions

Our present study shows that the $TiAl_3$ phase is metastable for titanium concentrations below 0.15 wt.%, but only in a small temperature range above the solidification temperature of aluminium. The direct correlation between the observation of this phase and the enhanced nucleation reveals that the duplex nucleation theory is the mechanism responsible for the grain refinement process in these alloys. After the formation of aluminium grains, the $TiAl_3$ phase subsequently dissolves at the expense of the more stable solid aluminium–titanium alloy. Our present experiments demonstrate that nucleation and growth of individual grains can be studied during solidification within the bulk of liquid metals. These in situ experiments offer the opportunity to validate the theoretical models widely used to predict the solidification process. This is of crucial importance to many industries that use grain refinement to produce solidified materials with favourable mechanical properties.

Acknowledgements

We acknowledge the European Synchrotron Radiation Facility for provision of synchrotron radiation facilities and we would like to thank G. Vaughan and A. Götz for assistance in using beamline ID11. We thank Y. Huang for assistance with the sample preparation. This work was financially supported in part by the Foundation for Fundamental Research on Matter (FOM) of the Netherlands Organisation for Scientific Research (NWO) and the Netherlands Institute for Metals Research (NIMR).

References

[1] Christian JW. The theory of transformations in metals and alloys. Oxford: Pergamon; 1981.
[2] Gasser U, Weeks ER, Schofield A, Pusey PN, Weitz DA. Science 2001;292:258.
[3] Auer S, Frenkel D. Nature 2001;409:1020.
[4] Lauridsen EM, Jensen DJ, Poulsen HF, Lienert U. Scripta Mater 2000;43:561.
[5] Margulies L, Winther G, Poulsen HF. Science 2001;292:2392.
[6] Larson BC, Yang W, Ice GE, Budal JD, Tischler JZ. Nature 2002;415:887.
[7] Offerman SE, van Dijk NH, Sietsma J, Grigull S, Lauridsen EM, Marguilies L, et al. Science 2002;298:1003.
[8] McCartney DG. Int Mater Rev 1989;34:247.
[9] Schumacher P, Greer AL, Worth J, Evans PV, Kearns MA, Fisher P, et al. Mater Sci Technol 1998;14:394.
[10] Easton M, StJohn D. Metall Mater Trans A 1999;30:1613.
[11] Easton M, StJohn D. Metall Mater Trans A 1999;30:1625.
[12] Kelton KF. Solid state physics, vol. 45. New York: Academic; 1991. p. 75.
[13] Maxwell I, Hellawell A. Acta Metall 1975;23:229.
[14] Zener C. J Appl Phys 1949;20:950.
[15] Ershov GS, Kasatkin AA, Golubev AA. Russ Metall 1978;2:62.
[16] Greer AL. Phil Trans R Soc Lond A 2003;361:479.